Extraordinary Infrared Transmission Resonances of Metal Microarrays for Sensing Nanocoating Thickness

Kenneth R. Rodriguez, Hong Tian, Joseph M. Heer, and James V. Coe*

The Ohio State University Department of Chemistry, 100 West 18th Avenue, Columbus, Ohio 43210-1173

Received: May 4, 2007; In Final Form: June 13, 2007

Nanocoatings of TiO_2 (60−105 nm in thickness) were applied to one side of freestanding Ni films with microarrays of subwavelength holes exhibiting the extraordinary transmission effect in the infrared. Shifts, attenuation, and broadening of the transmission resonances at perpendicular incidence have been observed versus coating thickness. The Ni microarrays exhibit potential as sensors for nanoscale coating thickness and dielectric properties, all of which are accomplished simply by placing mesh in the sample region of an FTIR spectrometer in transmission mode, at perpendicular incidence, without any angle tuning. A second order relation between resonance shifts and coating thickness has been developed which accounts for the effect of changing wavelength of this configuration. A framework is developed for converting these results to momentum space allowing comparison with surface plasmon attenuated total reflection experiments. This exercise illuminates the need for better theoretical models of radiation damping on mesh.

Introduction

Metal films with arrays of subwavelength holes (meshes) have unusual optical properties[1−4] including the extraordinary transmission effect[3,5] whereby more radiation is transmitted by the mesh than is incident upon its holes. This effect is mediated by surface plasmons (SPs) which can be thought of as light trapped at the metal surface by the "plasma" of conducting electrons in the metal. Metal array patterns offer a new (and fairly simple) way to integrate propagating SP optics into devices. In fact, double stacks of meshes present a way to get probing light of micrometer scale wavelengths into the nanoscale spaces[6] between meshes offering spectroscopic assays of such spaces not previously available. Meshes, with geometry as revealed by scanning electron microscope (SEM) images in Figure 1, can be placed in the sample region of standard Fourier transform infrared (FTIR) spectrometers at perpendicular incidence, producing SP-mediated transmission resonances (see the black trace in Figure 2) over the whole range of fundamental molecular vibrations. This constitutes a remarkably simple and broadly accessible way to excite SPs. The arrangement does not compromise the spectrometer optics or modulation schemes and can achieve >10 μm SP pathlengths (along the metal surface, perpendicular to the incident beam) that are useful for enhanced infrared (IR) absorption spectroscopy[5−14] which has been performed on self-assembled monolayers,[9,13,14] phospholipid bilayers,[6,9,14,15] and catalytic surface reactions.[9,11] The extraction of information from the mesh transmission resonances has been less explored by us but has the potential to quantify thickness and dielectric permittivity of nanoscale coatings, the topic of this paper.

The high dielectric constants of TiO_2 films[16,17] result in extensive interest regarding "thin-film capacitors, antireflection coatings, optical waveguides, photoelectrochemical cells, sensors, and mechanical or corrosion resistant barriers".[18,19] In this work, the effect of 60−105 nm thick coatings of TiO_2 on the zero-order IR transmission resonances at perpendicular incidence of Ni microarrays is presented. The predominant resonance exhibits red shifting, attenuation, and broadening as a function of TiO_2 coating thickness. Recognition of a special property of these meshes (the resonance splitting due to front−back coupling of SPs through the holes) enables these measurements at perpendicular incidence to be converted into shifts at specific wavelengths in momentum space, all without variation of the angle of the incident beam relative to the mesh. Again, this constitutes a simple and broadly accessible way to determine shifts in momentum space which may be directly compared to results for propagating SPs on smooth and thin metal films, that is, SP attenuated total reflection experiments (SP-ATR where fixed−wavelength laser intensity reflected from a metal-coated prism is monitored vs angle in search of SP reflection resonances[20−22]). Unlike the angle-scanned and wavelength-fixed SP-ATR experiments, wavelength-scanned and perpendicularly incident mesh experiments have resonance positions because of coating thickness at different wavelengths. There is a need to account for changing wavelength in order to calibrate for coating thickness, and we have developed an expression for the relation of coating thickness and mesh resonance position shifts based on Pockrand's second order SP-ATR theory for absorbing coatings.[23] The comparison of SP-ATR theory to mesh results illuminates the potential for obtaining complex dielectric permittivity of nanoscale mesh coatings and the importance of radiation damping (the process by which a propagating SP is turned back into a photon). Radiation damping is stronger on mesh arrays than with most SP-ATR experiments. The resonances most affected are also the most sensitive to nanocoatings. So there is a need for theoretical models of radiation damping on mesh (which is considerably different than radiation damping on thin metal films) in order to fully realize the potential for extracting explicit thickness and dielectric permittivity information of mesh nanocoatings from the shifts, attenuation, and broadening of mesh resonances in zero-order transmission spectra at perpendicular incidence.

---

* Corresponding author. E-mail: coe.1@osu.edu.

10.1021/jp073429m CCC: $37.00

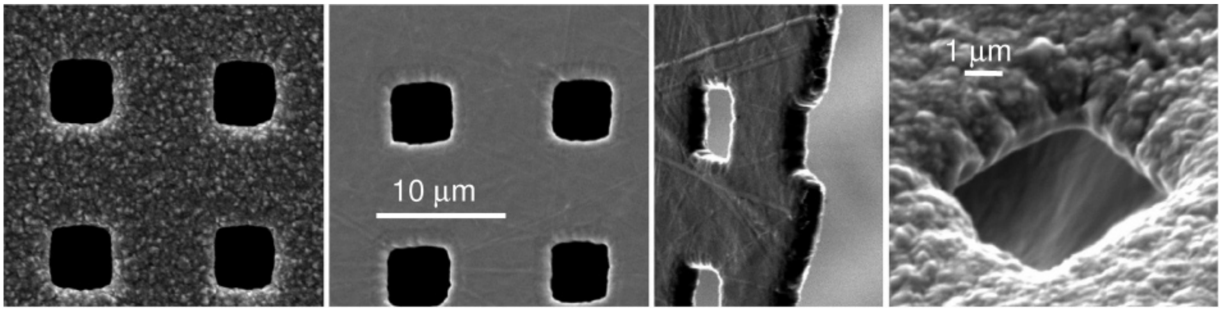

Figure 1. SEM images of the Ni microarrays with square holes on a square lattice. The mesh is made by Precision Eforming of Courtland, NY. The white bar is 10 μm for the first three images and 1 μm for the last image of a hole. The lattice parameter is 12.7 μm, the hole width is 5 μm, and the film width is ~3 μm (as shown in the third image from the right). One side of the freestanding mesh is rougher (first image) than the other side (second image).

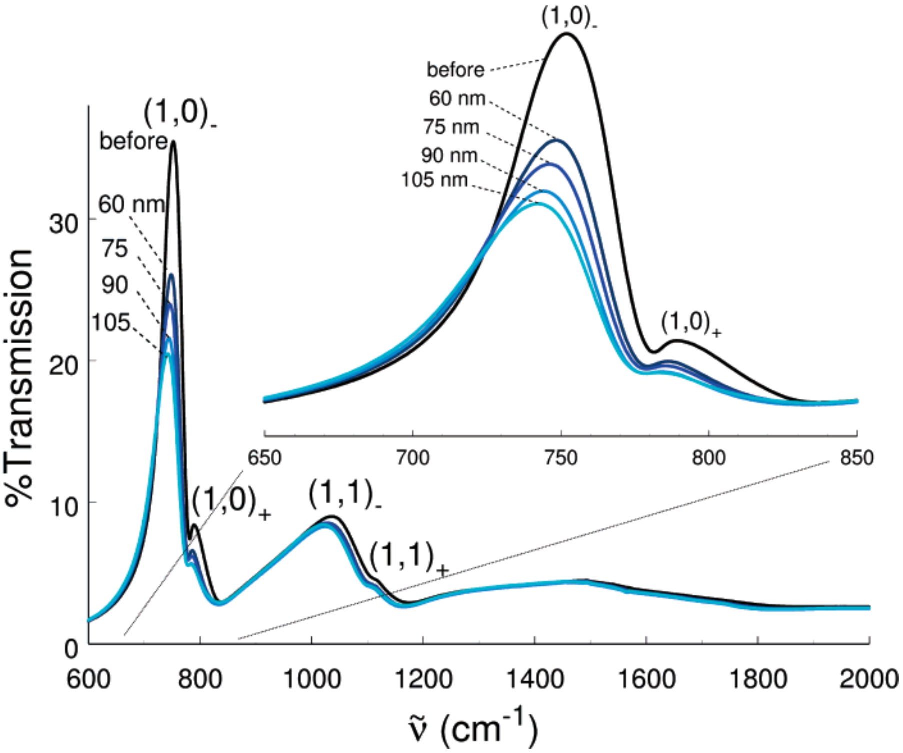

Figure 2. Zero-order transmission spectra at perpendicular incidence of the Ni mesh pictured in Figure 1 upon successive coatings with TiO_2. The $(1,0)_\pm$ resonance region is expanded in the inset so that the shifts, attenuation, and broadening of the $(1,0)_-$ resonance can be better discerned. The data were recorded in a Perkin-Elmer Spectrum GX FTIR spectrometer using 500 scans, at 4 cm^{-1} resolution, a DTGS detector, and unpolarized radiation.

Experimental Section

Nanocoatings of TiO_2 were applied to one side (the smooth side) of freestanding Ni films with microarrays of subwavelength holes (see Figure 1) that exhibit extraordinary IR transmission. These films are obtained from Precision Eforming. They only come in Ni and have a square lattice pattern of square holes (hole-to-hole spacing is 12.7 μm, the hole width is 5 μm, and the film thickness is ~3 μm). A Veeco/Telemark E-Beam evaporator was used at 4×10^{-6} Torr with a TiO_2 source to place TiO_2 films of 60−105 nm thickness on the Ni mesh. The thicknesses were determined by an adjacent quartz crystal capacitive microbalance with an uncertainty of ±2 nm. Zero-order, FTIR transmission spectra at perpendicular incidence are presented in Figure 2 for coatings with a thickness of 0, 60, 75, 90, and 105 nm (using a Perkin-Elmer Spectrum GX FTIR spectrometer, 500 scans, 4 cm^{-1} resolution, DTGS detector, and unpolarized radiation). The isolated resonance positions, full-width-at-half-maximum (fwhm), and intensities are given in Table 1. The resonance positions were determined both by polynomial interpolation at peak tops and by first derivative zero crossovers. Since both of the "+" resonances are small and the $(1,1)_+$ resonance is a shoulder, not a peak, both of the "+" resonances were isolated from their larger "−" partners by spline modeling of the "−" resonance wings in the vicinity of the smaller "+" resonances. The parameters determined in this manner are given in parentheses in Table 1.

Results

Resonance Response Before Coating. The transmission spectrum of the Ni mesh before coating (black trace in Figure 2) reveals two prominent resonances [labeled (1,0) and (1,1)], and each is split into a large and small peak (labeled with "+" or "−"). Resonance positions at perpendicular incidence with

TABLE 1: Transmission Resonance Peak Centers, FWHM, and Heights (% Transmission Relative to No Mesh in the Spectrometer) vs Thickness of the TiO_2 Nanocoating[a]

resonance coating	$(1,0)_-$	$(1,0)_+$	$(1,1)_-$	$(1,1)_+$
before				
center	752.0 cm^{-1}	789.3 cm^{-1}	1035.7 cm^{-1}	1117.8(1120.3) cm^{-1}
FWHM	43.4 cm^{-1}	(29.1) cm^{-1}	221 cm^{-1}	(22.1) cm^{-1}
height	35.5%	(2.0)%	9.0%	(0.31)%
60 nm				
center	748.4 cm^{-1}	786.1 cm^{-1}	1029.0 cm^{-1}	1115.3(1117.1) cm^{-1}
FWHM	50.4 cm^{-1}	(22.1) cm^{-1}	214 cm^{-1}	(26.4) cm^{-1}
height	26.1%	(0.68)%	8.5%	(0.20)%
75 nm				
center	746.2 cm^{-1}	785.2 cm^{-1}	1025.8 cm^{-1}	1114.6(1116.2) cm^{-1}
FWHM	53.1 cm^{-1}	(21.2) cm^{-1}	211 cm^{-1}	(28.2) cm^{-1}
height	24.0%	(0.81)%	8.5%	(0.23)%
90 nm				
center	744.2 cm^{-1}	784.0 cm^{-1}	1024.4 cm^{-1}	1113.7(1114.1) cm^{-1}
FWHM	55.5 cm^{-1}	(20.8) cm^{-1}	212 cm^{-1}	(24.7) cm^{-1}
height	21.6%	(0.53)%	8.3%	(0.18)%
105 nm				
center	742.2 cm^{-1}	783.1 cm^{-1}	1020.9 cm^{-1}	1113.1(1115.0) cm^{-1}
FWHM	58.9 cm^{-1}	(20.6) cm^{-1}	212 cm^{-1}	(28.3) cm^{-1}
height	20.5%	(0.43)%	8.4%	(0.19)%

[a] Quantities in parenthesis were determined upon isolating the resonance by subtracting a functional form for the larger nearby resonance.

a square lattice are given by the following relation based on surface momentum matching equations[6,10]

$$\tilde{\nu}_{(i,j)\pm} = \frac{\sqrt{i^2 + j^2}}{Ln'_{\mathrm{eff},\pm}} \tag{1}$$

where i and j identify the resonance by steps along the reciprocal lattice (essentially a diffraction spot no longer transmitted at this wavelength giving rise to surface waves), L is the lattice parameter or hole center to hole center spacing, and n'_{eff} is the real part of the effective index of refraction of the air/metal perforated interface. The splitting of each resonance (indicated by "+" or "−") is observable because the metal film thickness is a small fraction of the incident wavelength. It is due to the coupling of the propagating SPs between the front and the back surfaces of the mesh through the holes.[6,10,24,25] Knowledge of n'_{eff} is tantamount to knowledge of the SP dispersion curve in momentum space. The parameter $n'_{\mathrm{eff},+}$ is 1.000 in the IR for most smooth air/metal interfaces [based on $n'_{\mathrm{eff}} = \mathrm{Re}\{\sqrt{\epsilon_m\epsilon_s/(\epsilon_m+\epsilon_s)}\}$ where ϵ_m and ϵ_s are the complex dielectrics of the metal and substrate, respectively[22,23]]. It has also been determined to be 1.00 on mesh in air as revealed with an extensive dispersion study[10] by varying the angle of incident radiation on the mesh. Considering that Ni film is likely to have a thin oxide coating, we expect the SP_+ dispersion curve to be very close to the "light line" (the line on the dispersion diagram corresponding to light at parallel incidence to the surface). The position of the $(1,0)_+$ resonance at $\tilde{\nu}_{(1,0)+} = 789.3\ cm^{-1}$ and $n'_{\mathrm{eff},+} = 1.000$ determines, by eq 1, a value of $L = 12.7\ \mu m$ which is in agreement with SEM measurements. Furthermore, the ratio $\tilde{\nu}_{(1,1)+}/\tilde{\nu}_{(1,0)+}$ is 1.416 which is within 0.2% of the $\sqrt{2}$ as predicted by eq 1. So the behavior of propagating SPs on mesh is well described by eq 1. The "+" resonances are much less intense than the "−" resonances with our mesh geometries, but they serve as critical reference points for the conversion of frequency shifts of "−" resonances at perpendicular incidence to momentum space shifts for comparison to other SP work. On the other hand, the quantity $n'_{\mathrm{eff},-}$ can vary with wavelength, currently lacks good theoretical models on mesh, and is determined empirically in this work by the observed position of "−" resonances. The observed positions (Table 1) determine $n'_{\mathrm{eff},-}$ values [by $n'_{\mathrm{eff},-} = \sqrt{i^2+j^2}/(L\tilde{\nu}_{(i,j)-})$] of 1.050 at 752.0 cm^{-1} and 1.078 at 1035.7 cm^{-1} for the uncoated mesh. These values [along with 0 at 0 cm^{-1}] can be used to determine a working SP_- dispersion curve by fitting to simple functional forms. With these basics of uncoated mesh in hand, we proceed to the resonance behavior when the mesh is coated.

Resonance Response to Nanocoatings. The $(1,0)_-$ resonance (see Figure 2) shifts to lower frequencies, attenuates, and broadens with increasing thickness of TiO_2 nanocoatings. This is reminiscent of the absorbing coating response seen in SP-ATR results of Pockrand[26] as reviewed by Raether[22] (see Figure 2.1.7 therein), except that the mesh results are obtained at perpendicular incidence, without angling, and by scanning wavelength. The shift in resonance position before and after coating relative to the uncoated $(1,0)_+$ position is presented in Figure 3 for all of the resonances as a function of the TiO_2 coating thickness. Quadratic polynomial fits are given in Figure 3 as a guide to the eye. The "+" resonances display very similar shifts; however, the $(1,1)_+$ is a small shoulder with uncertainty comparable to its magnitude. All of the resonances respond to the coatings by shifting, but the "−" resonances show more response than the "+" resonances. The "−" resonances also have offsets without coatings (because of the front−back coupling of SPs through the holes) which are considerably larger than the coating shifts. The $(1,1)_-$ has the largest coating response, but it is a broad peak (fwhm $= \sim 220\ cm^{-1}$) that shows more scatter than the $(1,0)_-$ resonance (fwhm $= \sim 50\ cm^{-1}$). The $(1,0)_-$, which is also the most prominent resonance, would likely provide the best calibration curve for measuring the thickness of unknown TiO_2 nanocoating samples based on resonance position. A very thick coating (assuming anatase TiO_2) is roughly estimated to have a resonance occur at $\sim 135\ cm^{-1}$ [based on $n'_{\mathrm{eff}} = \mathrm{Re}\{\sqrt{\epsilon_m\epsilon_s/(\epsilon_m+\epsilon_s)}\}$], so there exists plenty of range with these experimental conditions for analyzing thicker coatings. Since our standard benchtop FTIR can measure positions of well-defined features to about 0.1 cm^{-1}, there is also potential (with more setup care and signal averaging) to characterize TiO_2 coating thicknesses in the 1−60 nm range. While the widths of the $(1,0)_+$ and $(1,1)_\pm$ resonances exhibit

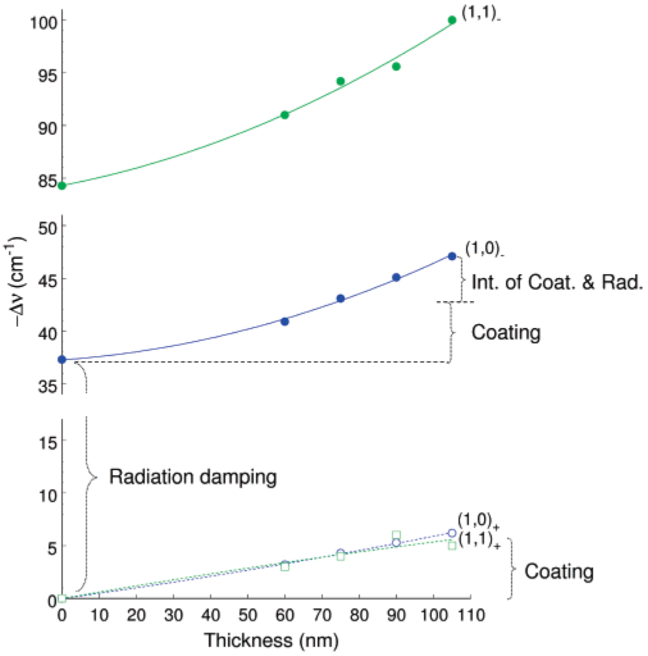

Figure 3. Shifts of transmission resonances vs thickness of TiO_2 coating relative to the uncoated position of the $(1,0)_+$ resonance. All of the resonances show response to coating thickness, but the "−" resonances show more response than the "+" resonances. The "−" resonances show large shifts without coating that is attributed to radiation damping associated with front−back coupling of SPs through the mesh holes. Note that the radiation damping shift is considerably larger than the shifts due to coating.

little response to coating thickness, the width of the $(1,0)_-$ resonance covers a range of fwhm from 43 cm^{-1} before coating to 59 cm^{-1} with the thickest TiO_2 coating (105 nm). By analogy to SP-ATR results,[22] the attenuation of this resonance and increase of its width are likely due to the imaginary component of the coating's dielectric permittivity, and the position shifting is largely due to the real component of the coating's dielectric permittivity. Consequently, these results demonstrate potential for measuring the complex dielectric permittivity of nanoscale coatings on mesh. The infrared SP resonances are clearly sensitive to the thickness and dielectric properties of nanoscale coatings of TiO_2, but unlike SP-ATR experiments, each resonance position of successively thicker coatings corresponds to a different wavelength. This is a difficulty that needs to be surmounted in order to determine thickness and dielectric permittivity from such results.

Determination of Shifts in Momentum Space. A dispersion diagram [$\tilde{\nu}$ (wavenumber) versus k_x (surface momentum wavevector along the holes)] for mesh before (blue) and after (green) coating is displayed in Figure 4. Zero-order transmission spectra at perpendicular incidence before (blue) and after (green) coating are shown on the left. In our arrangement, $k_x = 2\pi\tilde{\nu} \sin\theta$, where θ is the angle of the incident radiation from the surface normal along the direction of the holes. At perpendicular incidence, $k_x = 0$, and dots are used to indicate measured positions of the four transmission resonances. In order to compare to SP-ATR theory in the next section, we take $\tilde{\nu}_{(1,0)+}$ of the uncoated mesh (very close to $1/L$) as a reference point for resonance position shifts ($\Delta\tilde{\nu}$). Three types of shifts are depicted: the shift of the $(1,0)_+$ upon coating, the shift of the $(1,0)_-$ before coating, and the shift of the $(1,0)_-$ after coating. Surface momentum coupling comes in units of $2\pi/L$, so the measured resonance positions at $k_x = 0$ also correspond to points on SP dispersion curves at $k_x = 2\pi/L$. The SP dispersion curves are split into SP_+ and SP_- curves due to front−back SP coupling through the holes, and the SP_+ curve for uncoated mesh has been drawn close to the light line (without any surface oxide it would be right on the light line). Notice that the SP curves shift with coating (green lines) to a higher momentum wave vector (k_x). The diagram in Figure 4 shows how each frequency shift ($\Delta\tilde{\nu}$) corresponds to a shift (Δk_x) in momentum space. The shifts in this configuration are simply $\Delta k_x = 2\pi\Delta\tilde{\nu}$. Again, the real difficulty is that each Δk_x shift depicted in the diagram corresponds to a different value of $\tilde{\nu}$.

Comparison to SP-ATR Theory. We are now in a position to compare mesh results to those obtained in SP-ATR experiments. Pockrand has described second-order relations for the shifts in the complex SP momentum wave vector of SP-ATR work involving coatings of thin metal films on prisms.[23] In terms of shifts from the uncoated SP_+ curve, this is

$$\begin{aligned}\Delta \underline{k_x} &= (\text{coating}) + (\text{radiation damping}) + \\ &\quad (\text{interaction of coating and radiation damping}) \\ &= (\underline{k_x}^{(1)C} + \underline{k_x}^{(2)C}) + (\underline{k_x}^{(1)R} + \underline{k_x}^{(2)R}) + \underline{k_x}^{(2)CR} + \ldots\end{aligned} \tag{2}$$

where the bottom line uses Pockrand's notation and underlined quantities are complex. Pockrand gives explicit expressions for each of these terms as functions of thickness and dielectric permittivities of the coating, metal, and surrounding dielectrics. The quantity $\underline{k_x}^{(1)C} + \underline{k_x}^{(2)C}$ is the first and second order contribution to the shift due to the coating; the quantity $\underline{k_x}^{(1)R} + \underline{k_x}^{(2)R}$ is the first- and second-order contribution due to radiation damping, and $\underline{k_x}^{(2)CR}$ is a second-order term describing the interaction of the coating and radiation damping. Each of these terms can be seen in the shifts of Figure 3 and have been indicated in the figure for the (1,0) resonance. The term $\underline{k_x}^{(1)C} + \underline{k_x}^{(2)C}$ is given by 2π times the shifts of the "+" resonances (see the bottom two traces in Figure 3). Pockrand's explicit expressions may be directly applicable to these shifts (as will be presented shortly). The term $\underline{k_x}^{(1)R} + \underline{k_x}^{(2)R}$ is due to radiation damping and is given on the left side of Figure 3 at zero thickness by 2π times the shifts of the "−" resonances. In SP-ATR, radiation damping is due to the coupling of SPs on the two smooth metal/dielectric interfaces through the thin metal film. Pockrand's explicit radiation damping expressions are not applicable to mesh but indicate a type of theoretical modeling that would be very useful on mesh. Note that the radiation damping shift before coating of the mesh [2π(36 cm^{-1}) for the $(1,0)_-$ resonance and 2π(84 cm^{-1}) for the $(1,1)_-$ resonance] is considerably larger than the shifts of any of the resonances due to coating. Finally, the last term of eq 2, $\underline{k_x}^{(2)CR}$ (interaction of radiation damping and coating thickness), is exhibited in Figure 3 as the increase in response of the "−" resonances to coating thickness over that of the "+" resonances. The "+" resonances shift in momentum space by 2π(6 cm^{-1}) cm^{-1} with a 105 nm coating, while the $(1,0)_-$ shifts 2π(10 cm^{-1}) cm^{-1}, and the $(1,1)_-$ shifts 2π(15 cm^{-1}) cm^{-1}. Notice that the $\underline{k_x}^{(2)CR}$ term is comparably important to the $\underline{k_x}^{(1)C} + \underline{k_x}^{(2)C}$ term on mesh, again speaking to the greater importance of radiation damping.

Without a model for radiation damping on mesh, our only recourse for addressing dielectric properties is to use the shifts of the "+" resonances in spite of the fact that they are considerably less intense. Using complex dielectrics of the metal, coating, and surrounding medium as $\underline{\epsilon_m} = \epsilon'_m + i\epsilon''_m$, $\underline{\epsilon_c} = \epsilon'_c + i\epsilon''_c$, and $\underline{\epsilon_d} = \epsilon_d$, respectively, Pockrand's explicit expressions for $\underline{k_x}^{(1)C} + \underline{k_x}^{(2)C}$ can be rewritten using his prescription

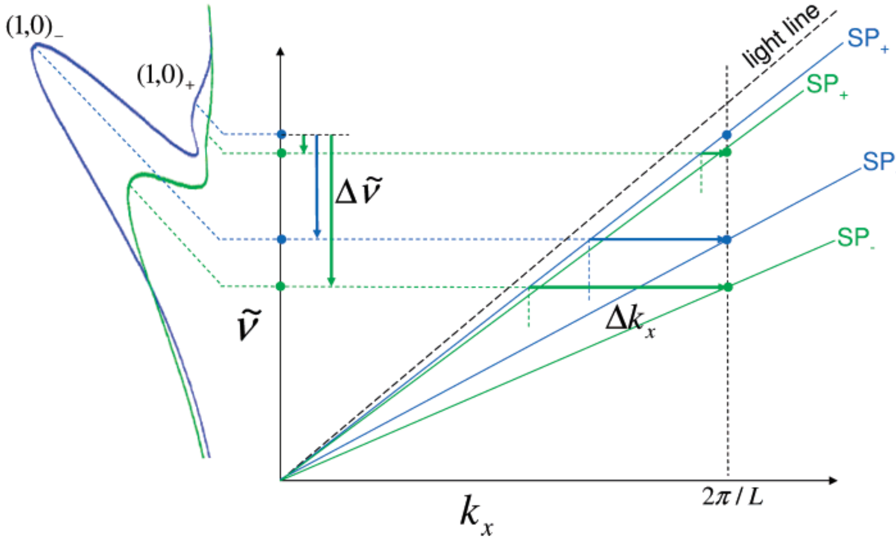

Figure 4. Dispersion diagram showing the conversion of shifts in frequency space ($\Delta\tilde{\nu}$) to shifts in momentum space (Δk_x) in order to facilitate the comparison to SP-ATR work. Transmission spectra before (blue) and after coating (green) are shown at left where peak positions correspond to points at $k_x = 0$ on the diagram. They are coupled to SP dispersion curves in units of $2\pi/L$ and therefore at $k_x = 2\pi/L$. The shifts in $\Delta\tilde{\nu}$ are all referenced to the uncoated SP_+ dispersion curve which lies very close to the light line. The conversion is simply $\Delta k_x = 2\pi\Delta\tilde{\nu}$, but the Δk_x shifts correspond to different values of $\tilde{\nu}$, unlike with SP-ATR work.

for absorbing coatings and collecting on coating thickness (d_c) as

$$\underline{k_x}^{(1)C} + \underline{k_x}^{(2)C} = \left(1 - i\frac{\epsilon_m}{2\epsilon'_m}\right)\underline{A}\tilde{\nu}^2 d_c + \frac{\underline{A}^2\underline{B}}{4\pi\sqrt{\dfrac{\epsilon'_m\epsilon_d}{\epsilon'_m + \epsilon_d}}}\tilde{\nu}^3 d_c^2 \quad (3)$$

where

$$\underline{A} = (2\pi)^2\left(\frac{\underline{\epsilon_c} - \epsilon_d}{\underline{\epsilon_c}}\right)\left(\frac{\epsilon'_m\epsilon_d}{\epsilon'_m + \epsilon_d}\right)^2\left(\frac{\underline{\epsilon_c} - \epsilon'_m}{\epsilon_d - \epsilon'_m}\right)(-\epsilon'_m\epsilon_d)^{-1/2} \quad (4)$$

$$\underline{B} = 2\frac{2\epsilon_d^2 - \underline{\epsilon_c}^2}{\epsilon_d(\epsilon_d - \underline{\epsilon_c})} + \frac{\epsilon'_m + \epsilon_d}{-\epsilon_d} \quad (5)$$

The shifts in frequency space at perpendicular incidence are just the real part of eq 3 divided by 2π. In the end, one obtains a simple and real working expression for the shifts of "+" resonances in frequency space for coating only as,

$$-\Delta\tilde{\nu} = C\tilde{\nu}^2 d_c + D\tilde{\nu}^3 d_c^2 \quad (6)$$

where C and D are the real parts of the corresponding terms in eq 3 divided by 2π. Accounting for wavelength change is quite important since $\tilde{\nu}$ occurs as a square and cube in the terms of eq 6. Equation 6 lays the foundation, or at least shows the feasibility, for using the shifts of mesh transmission resonances at perpendicular incidence to determine the thickness and dielectric properties of thin coatings. The $(1,0)_+$ shifts produce a reasonable fit to eq 6 giving

$$\Delta\tilde{\nu}_{(1,0)+} = (0.78 \pm 0.05)\tilde{\nu}^2 d_c + (24 \pm 7)\tilde{\nu}^3 d_c{}^2 \quad (7)$$

where $\Delta\tilde{\nu}$ and $\tilde{\nu}$ are in cm^{-1}, d_c is the thickness of the TiO_2 coating in cm (not nm), the uncertainties are estimated standard deviations (esd), and the esd of the fit is 0.1 cm^{-1}. There is a small (but unknown) shift due to the unavoidable NiO coating of a Ni mesh. In this case, the effect is additive because all of the results reported herein are on the same mesh with the same NiO thickness. But the total response is inherently nonlinear, so experiments with different NiO coatings may obtain different C and D fit parameters as defined in eqs 3−6. Note that the $(1,1)_+$ shifts have much greater uncertainty and did not yield an acceptable fit. While eq 6 clearly yields a useful empirical form, its direct validity is still under investigation.

The fit constants, C and D, can be calculated directly given dielectric values of the metal, coating, and surroundings. Direct application of the results in the preceding paragraph is impeded by the inevitable NiO coating that forms on the Ni mesh before TiO_2 coating. For example, the 6.2 cm^{-1} shift of the 105 nm TiO_2 coating can be simulated using eqs 3−6 and values of $\epsilon'_m = -150$ (for the effective Ni/NiO system), $\epsilon'_s = 35$ (an anatase value[19] for TiO_2), and $\epsilon_d = 1$, producing eq 6 constants (C and D) of 0.62 and 42 which are in the vicinity of the empirically fitted parameters. The 6.2 cm^{-1} shift of the 105 nm coating can also be simulated using values of $\epsilon'_m = -67$, $\epsilon'_s = 7$, and $\epsilon_d = 1$, producing eq 6 constants (C and D) of 0.76 and 24 which are very close to the empirical values. In both cases, the simulated ϵ'_m values are considerably smaller than the pure Ni value[29] of −1965 at 783.1 cm^{-1}. This suggests that the NiO layer and hole geometry produces an important reduction of the magnitude of Ni's dielectric value for the TiO_2 coatings, but work remains to determine if the simulated values are meaningful in some effective model. Without an NiO coating and fixing the metal and coating at the Ni and TiO_2 values, these equations predict only 2.0 cm^{-1} of red shift at a thickness of 105 nm, rather than the observed 6.2 cm^{-1}; so, the NiO coating may be enhancing (by as much as a factor of 3) the effect over bare metal (as is known for SiO_2 coatings[30] with coupled plasmon−wave guide resonators). Last, we observe that the magnitude of the second term in eq 6 is comparable to the first with 105 nm TiO_2 coatings; so, films of this thickness on our mesh lie just outside the linear region. That is, second order terms are important.

The "−" resonances are dramatically affected by radiation damping. Without a TiO_2 coating, the $(1,0)_-$ and $(1,1)_-$ resonances are shifted in frequency space by 37 and 84 cm^{-1}, respectively, from the corresponding "+" resonance. These values are considerably greater than the 6, 10, and 15 cm^{-1} changes observed for the $(1,0)_+$, $(1,0)_-$, and $(1,1)_-$ resonances, respectively, due to a 105 nm coating. The second term on the rhs of eq 2 for radiation damping, $\underline{k_x}^{(1)\text{R}} + \underline{k_x}^{(2)\text{R}}$, seems to be considerably larger on mesh than the first term, $\underline{k_x}^{(1)\text{C}} + \underline{k_x}^{(2)\text{C}}$, which is not typically the case with SP-ATR prism systems.

The greater sensitivity to coating thickness of the $(1,0)_-$ curve (see Figure 3) versus the $(1,0)_+$ curve is likely due to the interaction of coating and radiation damping, that is, the third term on the rhs of eq 2, $\underline{k_x}^{(2)\text{CR}}$. In order to characterize this type of interaction, the shifts in the $(1,0)_-$ resonance positions from their uncoated position were also fit to the form of eq 6 giving

$$\tilde{\nu}_{(1,0)-,\text{coated}} - \tilde{\nu}_{(1,0)-,\text{uncoated}} = (0.74 \pm 0.07)\tilde{\nu}^2 d_\text{c} + (118 \pm 11)\tilde{\nu}^3 d_\text{c}^2 \quad (8)$$

with a fit esd of 0.17 cm^{-1}. The enhancement in the response of the $(1,0)_-$ resonance due to the interaction of radiation damping and coating (over coating alone) is given by the difference between eqs 8 and 7 which is $(0.04 \pm 0.09)\tilde{\nu}^2 d_\text{c} + (86 \pm 13)\tilde{\nu}^3 d_\text{c}^2$. The first term is essentially zero suggesting that higher order terms of radiation damping are responsible for the enhancement in sensitivity to coating.

Conclusions

TiO_2 coatings in the 60−105 nm range of thickness produce changes in the positions of transmission resonances of Ni microarrays with thin NiO coatings that can easily be measured in FTIR spectrometers. The positions of the "+" resonances have been modeled with the same theory used for SP-ATR experiments excepting the radiation damping parts. The Ni mesh arrays display much stronger radiation damping than their SP-ATR coated prism counterparts, and on mesh, this renders greater sensitivity to TiO_2 nanocoatings for the "−" resonances. It is hoped that this work will compel some theoretical modeling of the relation of radiation damping on mesh to the dielectric properties of coatings. The FTIR transmission method has potential to measure thinner films than studied herein; however, protocols may have to be developed to keep the free-standing mesh flat and more reproducibly oriented at perpendicular incidence (such variations are about the same size as the observed shifts of thinner coatings). It seems that the NiO coating on the Ni mesh is important for optimal sensitivity to coatings; so, it will be important in the future to use a known and optimal thickness of NiO. Potential has been demonstrated for the determination of the thickness and complex dielectric constants of coatings on metal microarrays using FTIR spectrometer measurements of transmission resonances.

Acknowledgment. We thank the National Science Foundation for support of this work under Grant CHE-0413077 and the ACS PRF under Grant 42452-AC5.

References and Notes

(1) Dintinger, J.; Degiron, A.; Ebbesen, T. W. *MRS Bulletin* **2005**, *30*, 381.

(2) Barnes, W. L.; Dereux, A.; Ebbesen, T. W. *Nature (London)* **2003**, *424*, 824.

(3) Ebbesen, T. W.; Lezec, H. J.; Ghaemi, H. F.; Thio, T.; Wolff, P. A. *Nature (London)* **1998**, *391*, 667.

(4) Genet, C.; Ebbesen, T. W. *Nature (London, U. K.)* **2007**, *445*, 39.

(5) Williams, S. M.; Stafford, A. D.; Rodriguez, K. R.; Rogers, T. M.; Coe, J. V. *J. Phys. Chem. B* **2003**, *107*, 11871.

(6) Teeters-Kennedy, S. M.; Williams, S. M.; Rodriguez, K. R.; Cilwa, K.; Meleason, D.; Sudnitsyn, A.; Hrovat, F.; Coe, J. V. *J. Phys. Chem. C* **2007**, *111*, 124.

(7) Rodriguez, K. R.; Tian, H.; Heer, J. M.; Teeters-Kennedy Coe, J. V. *J. Chem. Phys.* **2007**, *126*, 151101.

(8) Teeters-Kennedy, S. M.; Rodriguez, K. R.; Rogers, T. M.; Zomchek, K. A.; Williams, S. M.; Sudnitsyn, A.; Carter, L.; Cherezov, V.; Caffrey, M.; Coe, J. V. *J. Phys. Chem. B* **2006**, *110*, 21719.

(9) Coe, J. V.; Williams, S. M.; Rodriguez, K. R.; Teeters-Kennedy, S.; Sudnitsyn, A.; Hrovat, F. *Anal. Chem.* **2006**, *March 1*, 1385.

(10) Williams, S. M.; Coe, J. V. *Plasmonics* **2006**, *1*, 87.

(11) Williams, S. M.; Rodriguez, K. R.; Teeters-Kennedy, S.; Stafford, A. D.; Bishop, S. R.; Lincoln, U. K.; Coe, J. V. *J. Phys. Chem. B* **2004**, *108*, 11833.

(12) Williams, S. M.; Stafford, A. D.; Rogers, T. M.; Bishop, S. R.; Coe, J. V. *Appl. Phys. Lett.* **2004**, *85*, 1472.

(13) Rodriguez, K. R.; Shah, S.; Williams, S. M.; Teeters-Kennedy, S.; Coe, J. V. *J. Chem. Phys.* **2004**, *121*, 8671.

(14) Williams, S. M.; Rodriguez, K. R.; Teeters-Kennedy, S.; Shah, S.; Rogers, T. M.; Stafford, A. D.; Coe, J. V. *Nanotechnology* **2004**, *15*, S495.

(15) Teeters-Kennedy, S. M. The Extraordinary Transmission of Subwavelength Metallic Arrays: An Infrared Study of the Self-Assembly of Phospholipid Bilayers on Alkanethiol Monolayers. M.S. Thesis, The Ohio State University, 2004.

(16) Park, J.-J.; Lee, W.-J.; Lee, G.-H.; Kim, I.-S.; Shin, B.-C.; Yoon, S.-G. *Integr. Ferroelectr.* **2004**, *68*, 129.

(17) Ha, H.-K.; Yoshimito, M.; Koinuma, H.; Moon, B.-K.; Ishiwara, H. *Appl. Phys. Lett.* **1996**, *68*, 2965.

(18) Ha, H.-K.; Yoshimoto, M.; Koinuma, H. *Appl. Phys. Lett.* **1996**, *68*, 2965.

(19) Kim, S. K.; Kim, W.-D.; Kim, K.-M.; Hwang, C. S.; Jeong, J. *Appl. Phys. Lett.* **2004**, *85*, 4112.

(20) Otto, A. *Z. Phys.* **1968**, *216*, 398.

(21) Kretschmann, E.; Raether, H. *Z. Naturforsch., A: Astrophys., Phys. Phys. Chem.* **1968**, *23*, 2135.

(22) Raether, H. *Surface plasmons on smooth and rough surfaces and on gratings*; Springer-Verlag: Berlin, 1988.

(23) Pockrand, I. *Surf. Sci.* **1978**, *72*, 577.

(24) Economou, E. N. *Phys. Rev.* **1969**, *182*, 539.

(25) Welford, K. R.; Sambles, J. R. *J. Mod. Opt.* **1988**, *35*, 1467.

(26) Pockrand, I.; Raether, H. *Appl. Opt.* **1977**, *16*, 1784.

(27) Yang, F.; Bradberry, G. W.; Sambles, J. R. *J. Mod. Opt.* **1990**, *37*, 993.

(28) Fuzi, Y.; Bradberry, G. W.; Sambles, J. R. *J. Mod. Opt.* **1989**, *36*, 1405.

(29) Rakic, A. D.; Djurisic, A. B.; Elazar, J. M.; Majewski, M. L. *Appl. Opt.* **1998**, *37*, 5271.

(30) Salamon, Z.; Macleod, H. A.; Tollin, G. *Biophys. J.* **1997**, *73*, 2791.